ILD benchmark: tau tau at 500 GeV

Daniel Jeans, Keita Yumino

March 27, 2019

Abstract

Analysis of $ee \to \tau\tau$ for detector benchmarking.

1 Introduction

Di-tau production at high COM. Polarisation of tau lepton is reconstructable thanks to its relatively short lifetime and "clean" decays.

We study the selection of such events and how their spin can be reconstructed. We compare the results in the two ILD detector models (large and small).

2 What we need to measure

The tau decay gives us sensitivity to its spin, and therefore to the left and right handed couplings of whatever intermediate particle produced them. In the $ee \to \tau\tau$ process, we plot the scattering angle and tau-tau invariant mass in Fig.1. These are shown at MC level, separately for samples with (100%) eLpR and eRpL beam polarisations.

We also plot the "exact" polarimeters in the case of $\tau^\pm \to \pi^\pm\nu$ and $\tau^\pm \to \pi^\pm\pi^0\nu$ decays. The polarimeter vectors are defined in the tau rest frames as follows: for $\tau^\pm \to \pi^\pm\nu$, it is the direction of the neutrino momentum, while for $\tau^\pm \to \pi^\pm\pi^0\nu$ it is the direction of the vector $\mathbf{P} = 2(\mathbf{q}\cdot\mathbf{p}_\nu)\mathbf{q} - m_q^2\mathbf{p}_\nu$, where $\mathbf{q} = \mathbf{p}_{\pi^\pm} - \mathbf{p}_{\pi^0}$, and $\mathbf{p}_\nu, \mathbf{p}_{\pi^\pm}, \mathbf{p}_{\pi^0}$ are respectively the 3-momenta of the neutrino, charged and neutral pions. To distinguish taus of different helicity, we look at the cosine of the angle this polarimeter vector makes to the tau flight direction.

It proves difficult to reconstruct the polarimeter in the case of rho decays in the di-tau event topology at these high energies (although this may be possible with further study). For the time being, we therefore adopt an approach which makes use of only the visible 4-vectors of the charged and neutral pions produced in rho decay, integrating over possible neutrino configurations, as described in [1]. The resulting "approximate" polarimeters are compared with the "exact" ones in figures 2 and 3 respectively for $\tau^\pm \to \pi^\pm\nu$ and $\tau^\pm \to \pi^\pm\pi^0\nu$ decays.

The aim of this analysis is essentially to see how well we can reconstruct these distributions in the large and small ILD models.

3 Event selection

It is the semi-leptonic tau decays (in which the tau decays to a single neutrino plus hadrons) which are most sensitive to tau polarisation (fully leptonic modes suffer from the presence of 2 neutrinos per tau decay). We therefore emphasise hadronic decays, in particular $\tau^\pm \to \pi^\pm\nu$ (the cleanest hadronic decay) and $\tau^\pm \to \pi^\pm\pi^0\nu$ (which has the largest decay branching ratio, accounting for around 26% of tau decays). These two decay modes both allow full extraction of polarisation information. We concentrate our efforts on events in which the tau pair invariant mass is close to the nominal collision energy of 500 GeV.

From the detector point of view, the identification and measurement of the charged hadron is rather easy. The most sensitive aspect is probably the reconstruction and measurement of the π^0 decay products in the highly boosted tau decays.

We first apply a simple preselection, requiring that between 2 and 12 charged PFOs have been reconstructed, to remove the majority of events with hadronic jets. We then look for two seed directions around which to build tau jet candidates. We identify the highest momentum charged PFO in the event ("first seed"). Once this has been found, we look for the next highest momentum charged PFO which is separated from the first seed by at least $\pi/2$ in the $x-y$ plane ($\delta\phi$). This selection makes use of the property that the two taus in signal events are emitted back-to-back in the $x-y$ plane in the case of collinear (or no) ISR. If no second seed is found, the event is rejected.

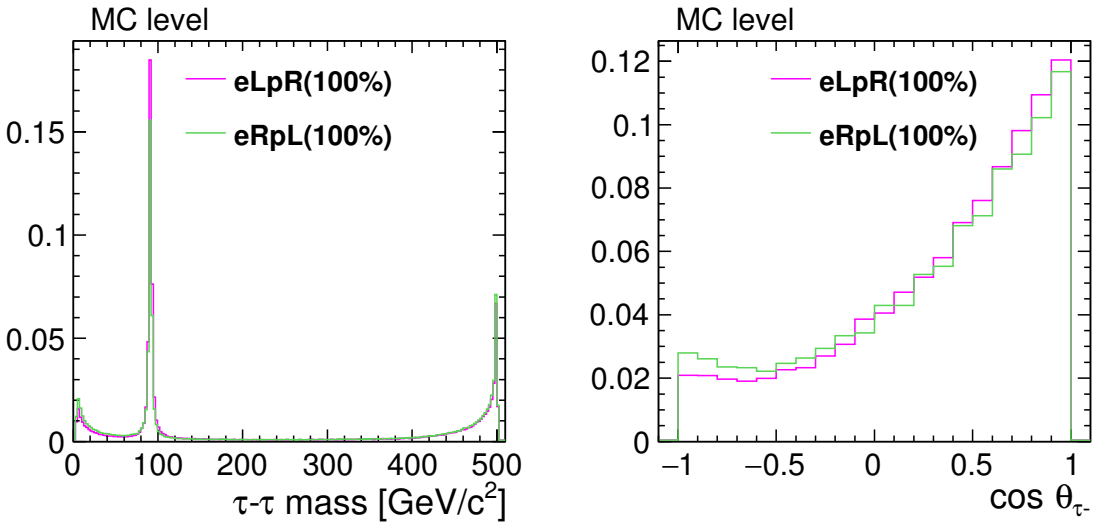

Figure 1: MC distributions. mtautau, and costhtau for events with $m_{\tau\tau} > 480$ GeV.

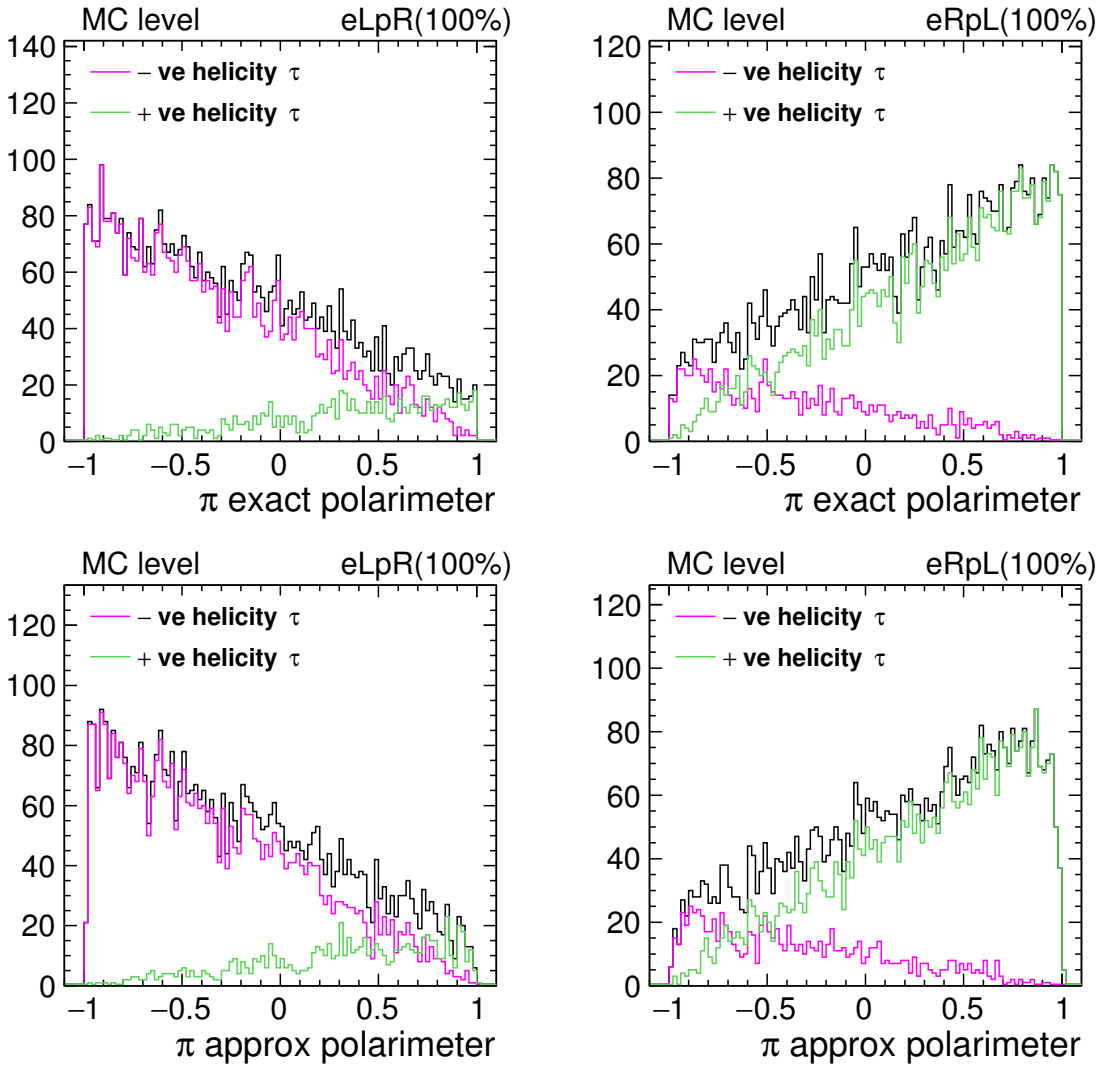

Figure 2: MC distributions. Pi polarimeters, for events with$m_{\tau\tau} > 480$ GeV.

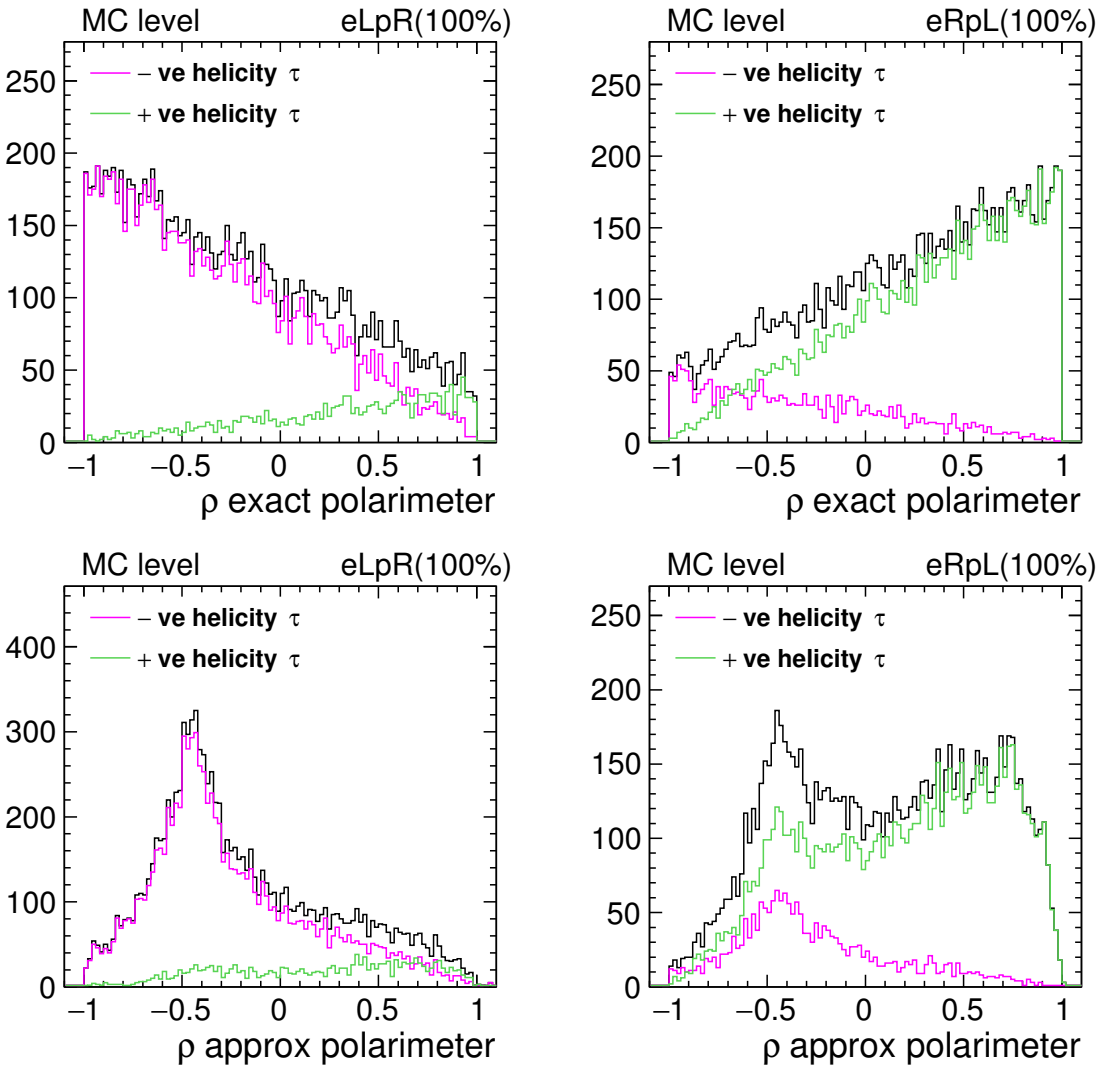

Figure 3: MC distributions. Rho polarimeters for events with $m_{\tau\tau} > 480$ GeV.

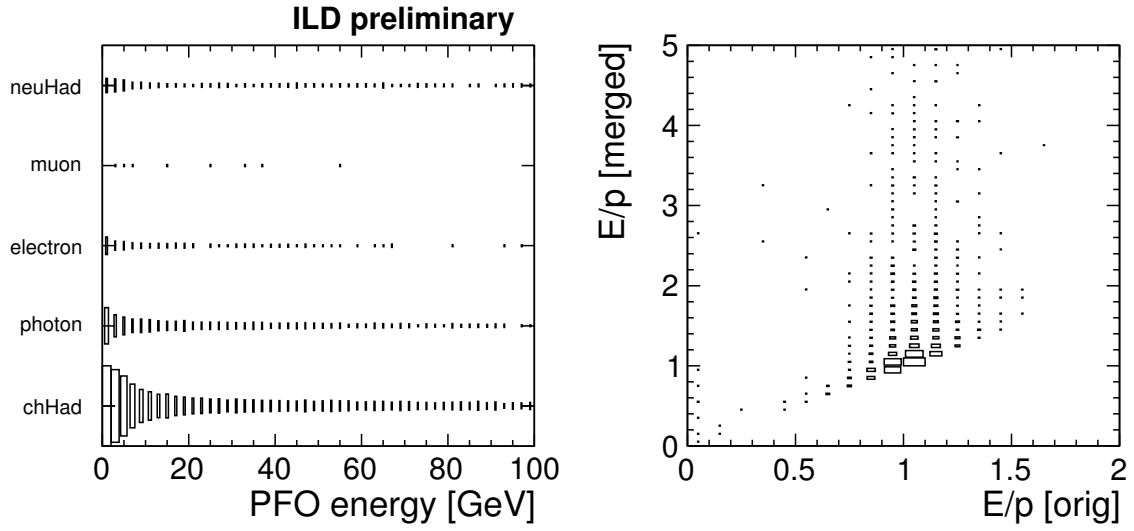

Figure 4: Left: the nature of the MC particle which created PFOs flagged as neutral hadrons, as a function of PFO energy. Right: Events with one charged hadron and one one neutral hadron: the E/p of the charged hadron before and after adding the neutral hadron cluster energy to it.

We then look in narrow cones (opening angle 0.1 rad) around these two seed directions. PFOs within these cones are associated to tau jet candidates. The cluster associated to each seed particle is modeled as an ellipsoid, of which the length (ie the length of the longest axis) and the "radius" (defined as the quadratic sum of the two smaller eigenvalues). We then apply the following selection:

- Energy of the second seed less than 200 GeV. [to remove di-lepton events.]
- Sum of the energy (p_T) of particles lying outside the two cones less than 40 (20) GeV. [remove hadronic events.]
- acoplanarity between candidate jet directions less than 0.05 rad. [remove fully leptonic WW events]
- acolinearity between candidate jet directions less than 0.075 rad. [remove Z return events.]
- No photon-like PFO (as tagged by PandoraPFA) with energy larger than 10 GeV lying outside the two cones. [remove events with seen ISR]
- No isolated leptons identified by the IsolatedLeptonTaggingProcessor. [remove dilepton events, fully leptonic tau decays]
- The energy-weighted shape of the cluster associated with each seed is modeled as an ellipsoid, the largest eigenvalue of which must be in the range 10 and $10^{3.6}$ mm, and the smallest between $10^{1.6}$ and $10^{4.0}$ mm.

We then look in more detail at the two jet cones. We observe that neutral hadrons are often reconstructed within the cones. This is almost always the result of fragmentation of the calorimetric shower induced by a charged hadron. The number of long-lived neutral hadrons produced in tau decays is rather small, so we remove such neutral hadron PFOs from the event. In Fig. 4, we look at the parent particle of those clusters flagged as neutral hadrons: the majority are due to fragmentation of the charged hadron. In the same figure we compare the E/p of the original charged hadron PFO, and what we obtain when the neutral hadron energy is added: the E/p is degraded (i.e. further from 1.0) when the neutral hadron is added: this helps understand why the reconstruction algorithm chooses to split off part of the hadronic shower into a distinct PFO.

If the total charge of the jet is zero, we remove the charged particle furthest from the jet's initial seed direction. After removing these PFOs from consideration, we calculate the invariant mass of the jet. We ask that this mass is less than 1.77 GeV, and also that the produce of the two jets' charges is -1.

Fig 5 shows the reasons that only a single photon cluster is sometimes found in rho decays:

- "converted": at least one photon converted in the tracking region;
- "noPFO (lowen)": no PFO associated with the photon was found (and at least one photon energy ¡ 300 MeV);
- "noPFO (other)": no PFO associated with the photon was found (and both photon energies ¿ 300 MeV);

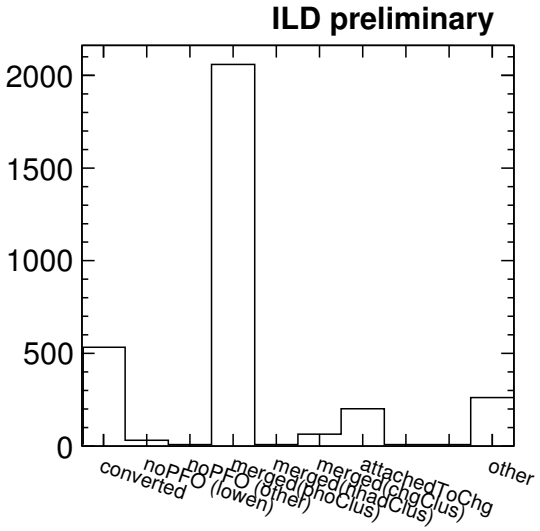

Figure 5: Reason for which only a single photon PFO was found in $\tau \to \rho$ decays. (see text for details.)

final state	$ee \to \tau\tau$			2f	4f
	SIGNAL		OTHER		
	efficiency [%]	expected events/1000			
original	100.0	219.2	5216.6	36801.1	51915.0
preselected	89.1	195.2	4517.4	7540.4	16236.3
two seeds	88.7	194.6	4281.3	7205.4	14338.8
out-of-cone activity	84.4	185.0	2437.3	1707.3	5887.0
acolinearity	83.0	181.9	1841.5	1116.3	713.0
acoplanarity	77.3	169.5	345.3	6.3	123.1
ISR veto	75.5	165.4	329.7	6.0	117.1
isolated lepton veto	74.7	163.9	238.7	4.9	28.6
seed cluster shape	65.6	143.8	24.9	3.6	2.1
candidate jet mass	56.4	123.7	17.4	0.3	1.4
jets' charge	54.6	119.6	16.5	0.1	1.3

Table 1: Selection efficiencies and expected event numbers at different stages of the selection (see text for details). Large detector, 1.8 ab-1 in the eLpR polarisation. SIGNAL refers to $ee \to \tau\tau$ events with $\tau\tau$ invariant mass greater than 480 GeV, and in which both τs decay hadronically.

- "merged (phoClus)": the two photons were attached to the same photon PFO;
- "merged (nhadClus)": the two photons were attached to the neutral hadron PFO;
- "merged (chgClus)": the two photons were attached to the same charged hadron PFO;
- "attachedToChg": one photon was attached to a charged hadron PFO;

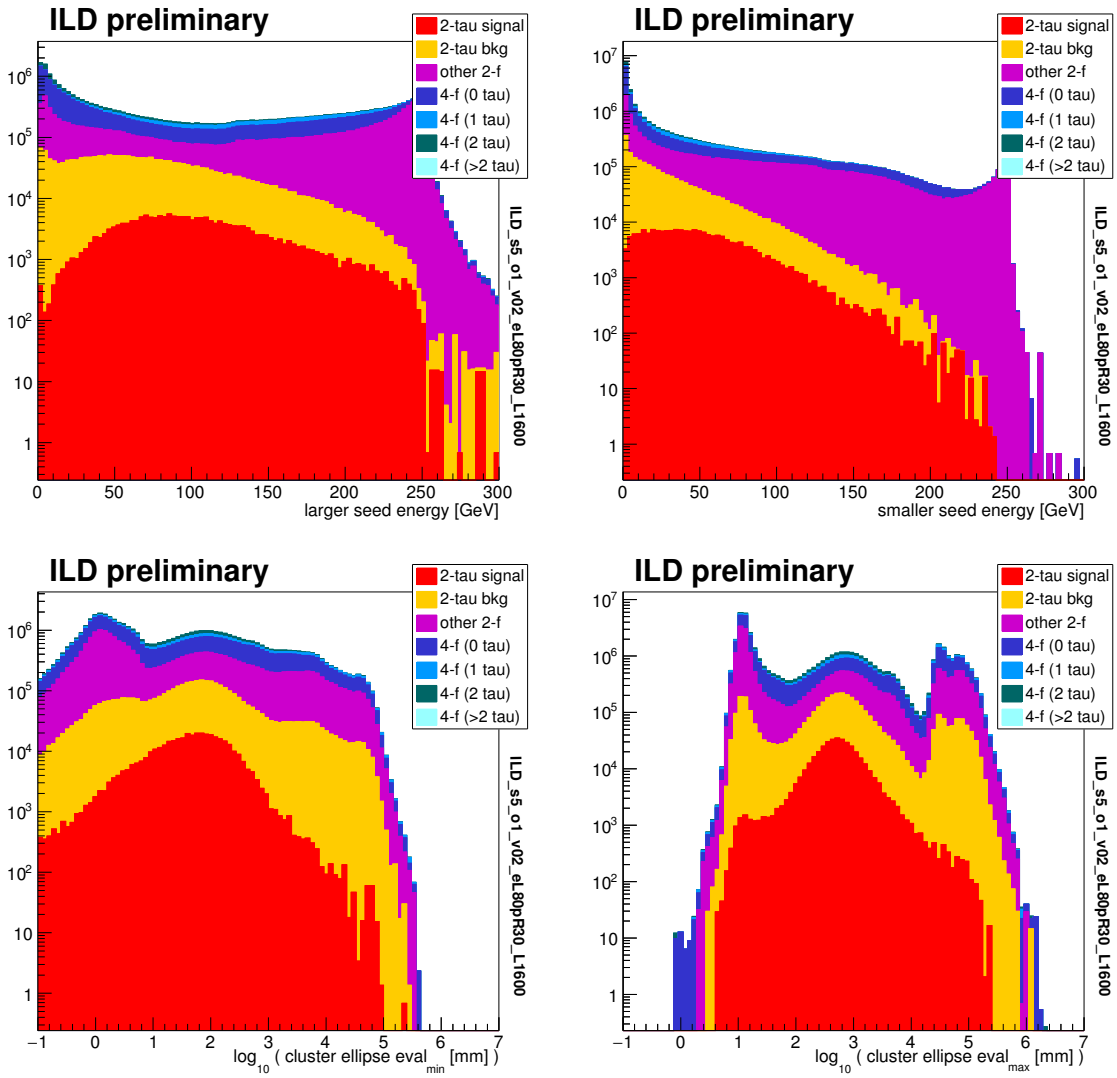

Figure 6: Distributions after preselection. The larger and smaller of the seed PFOs' energies, and the smaller and larger of the seeds' associated calorimeter cluster shape eigenvalues.

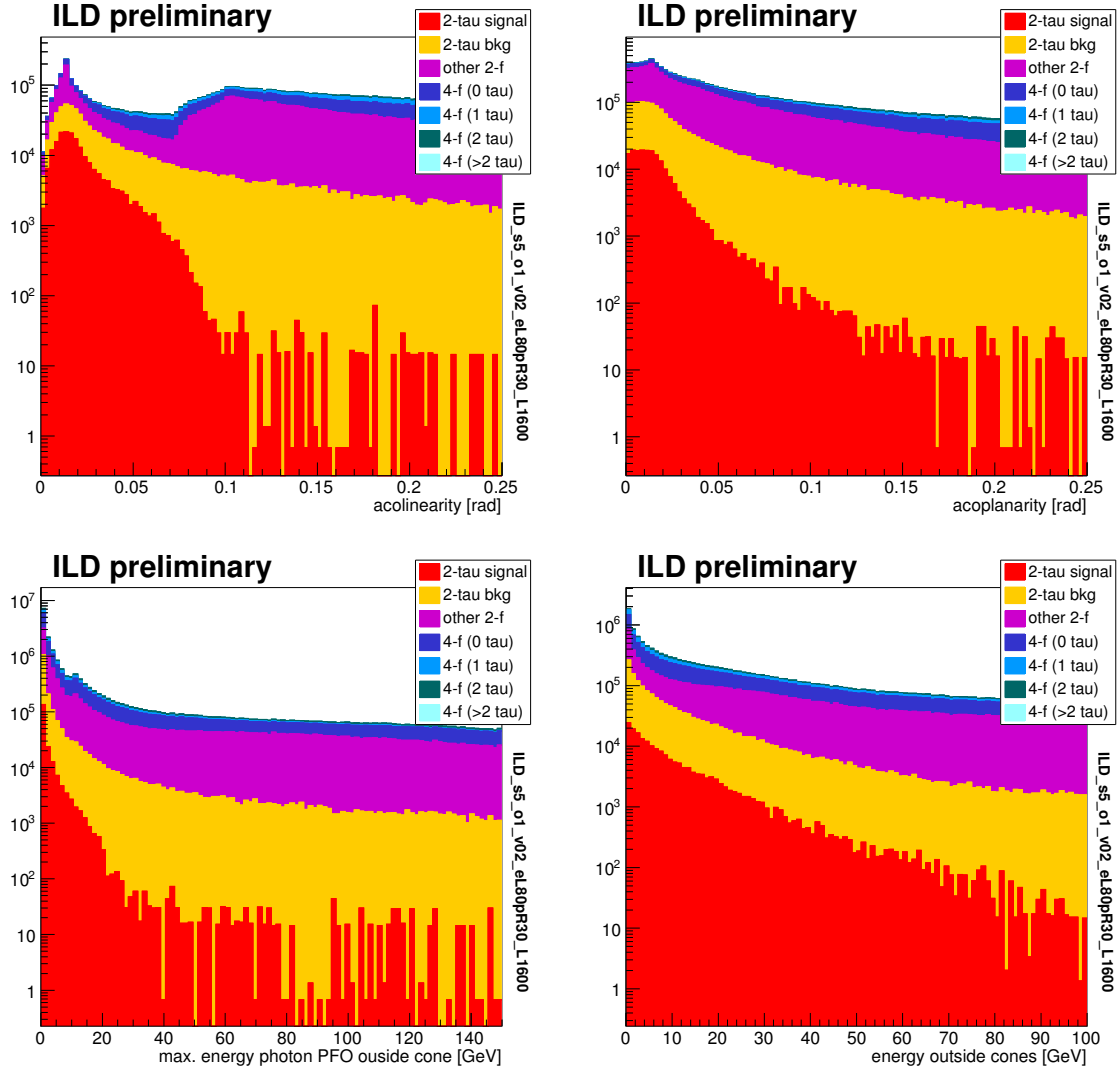

Figure 7: Distributions after preselection. Acolinearity and acoplanarity of the two candidate jets, the energy of most energetic photon PFO found outside the two jet cones, and the sum of the energy of all particles outside the cones.

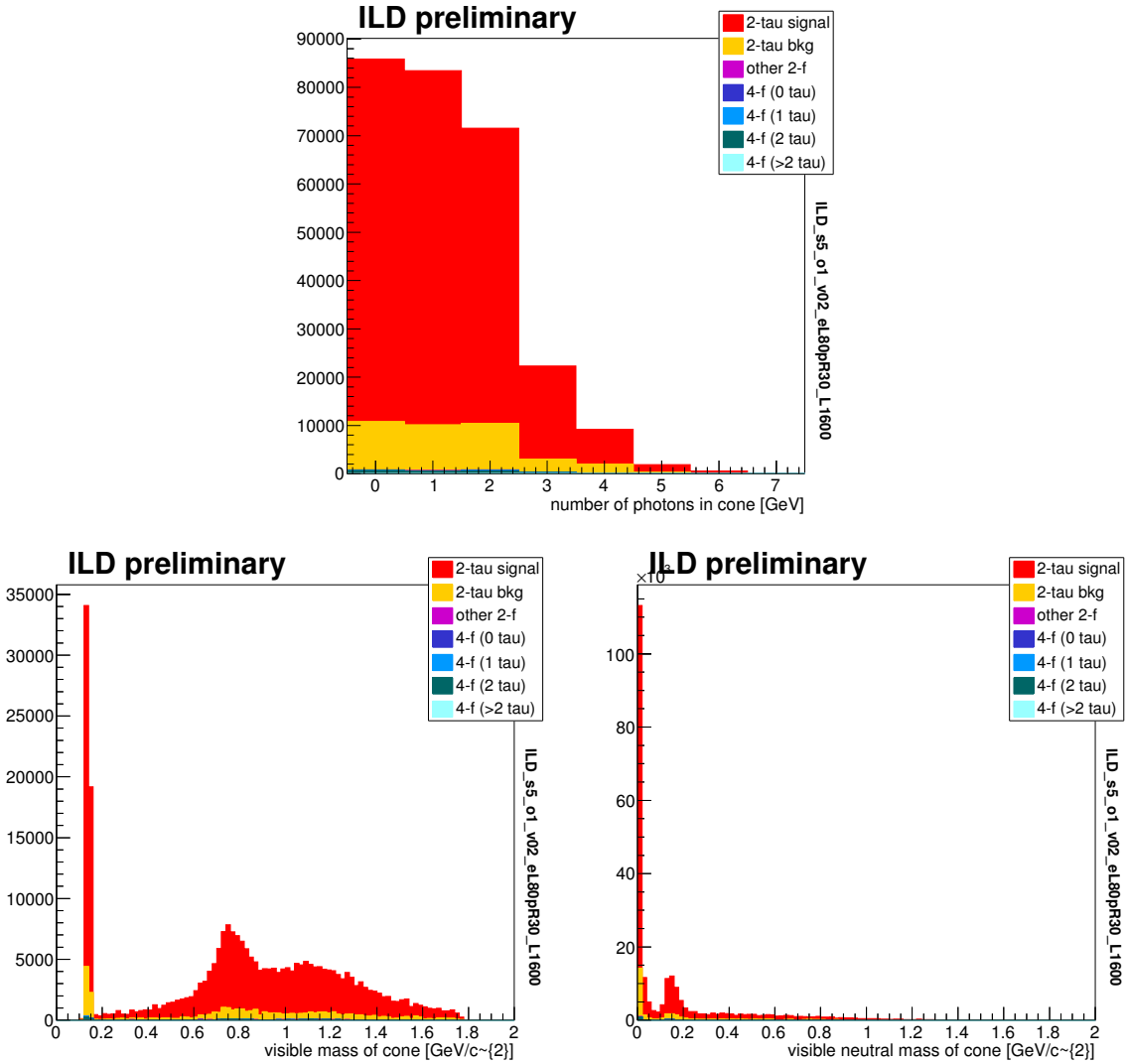

Figure 8: Distributions after preselection. The number of photon PFOs found per candidate jet, and the invariant mass of all (neutral) PFOs inside the jet.

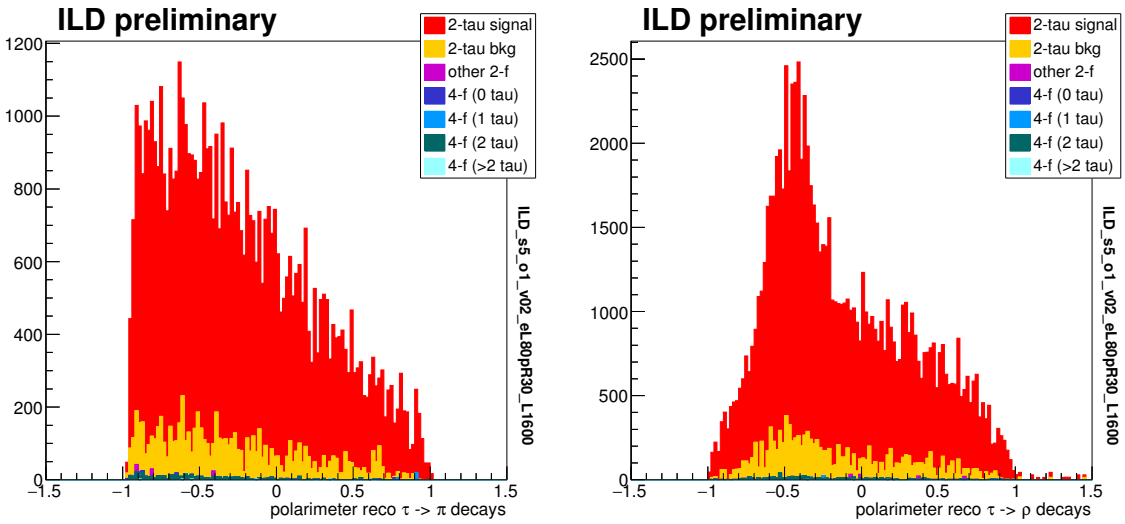

Figure 9: Distributions after preselection. Reconstructed polarimeters in jets identified as $\tau \to \pi, \rho$ decays.

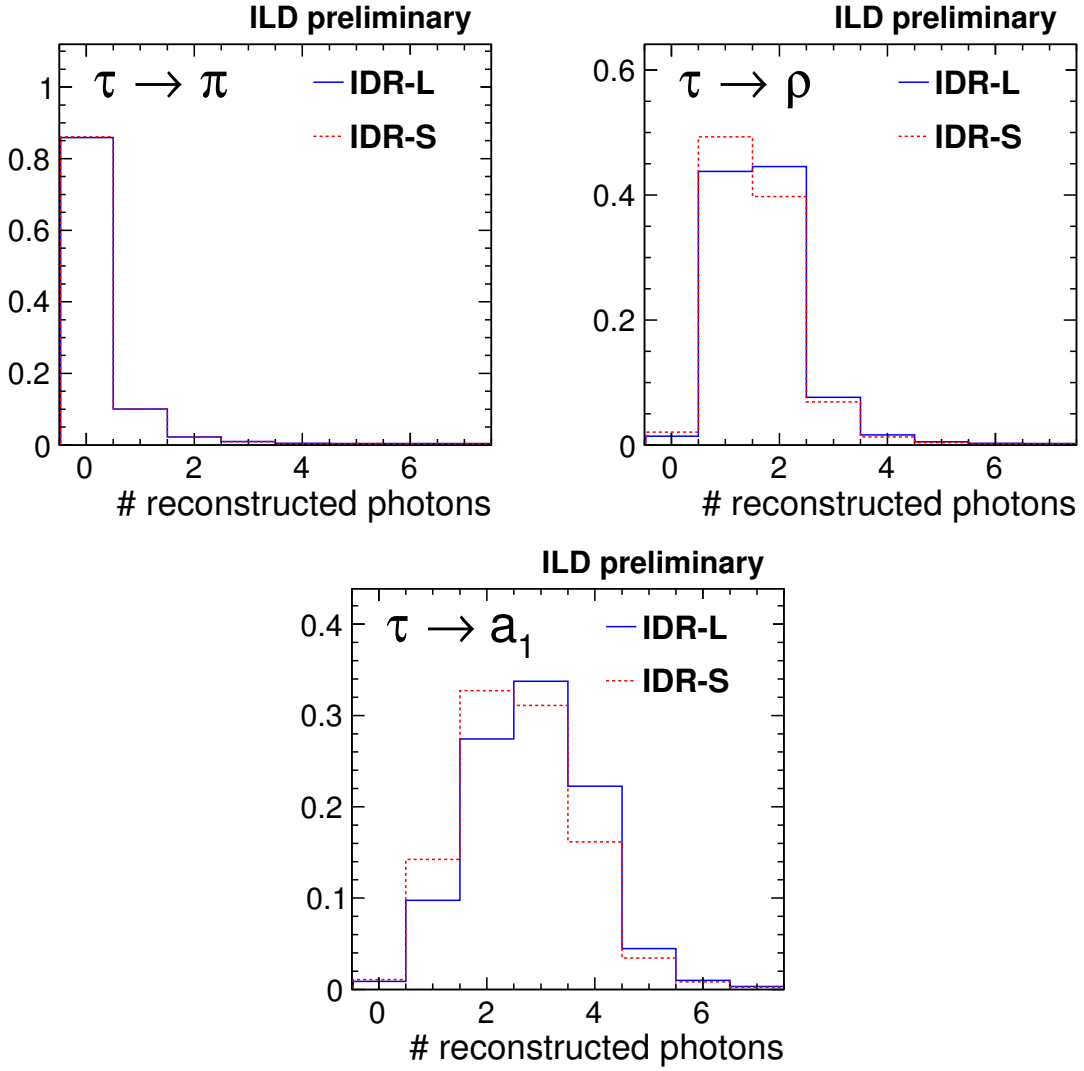

Figure 10: Signal-only comparisons after general event selection: the number of reco photons in candidate jets matched to taus decaying in the single pion, rho, and single-prong a1 modes. The expected number of photons produced in these decays is respectively 0, 2, and 4 in these decay models.

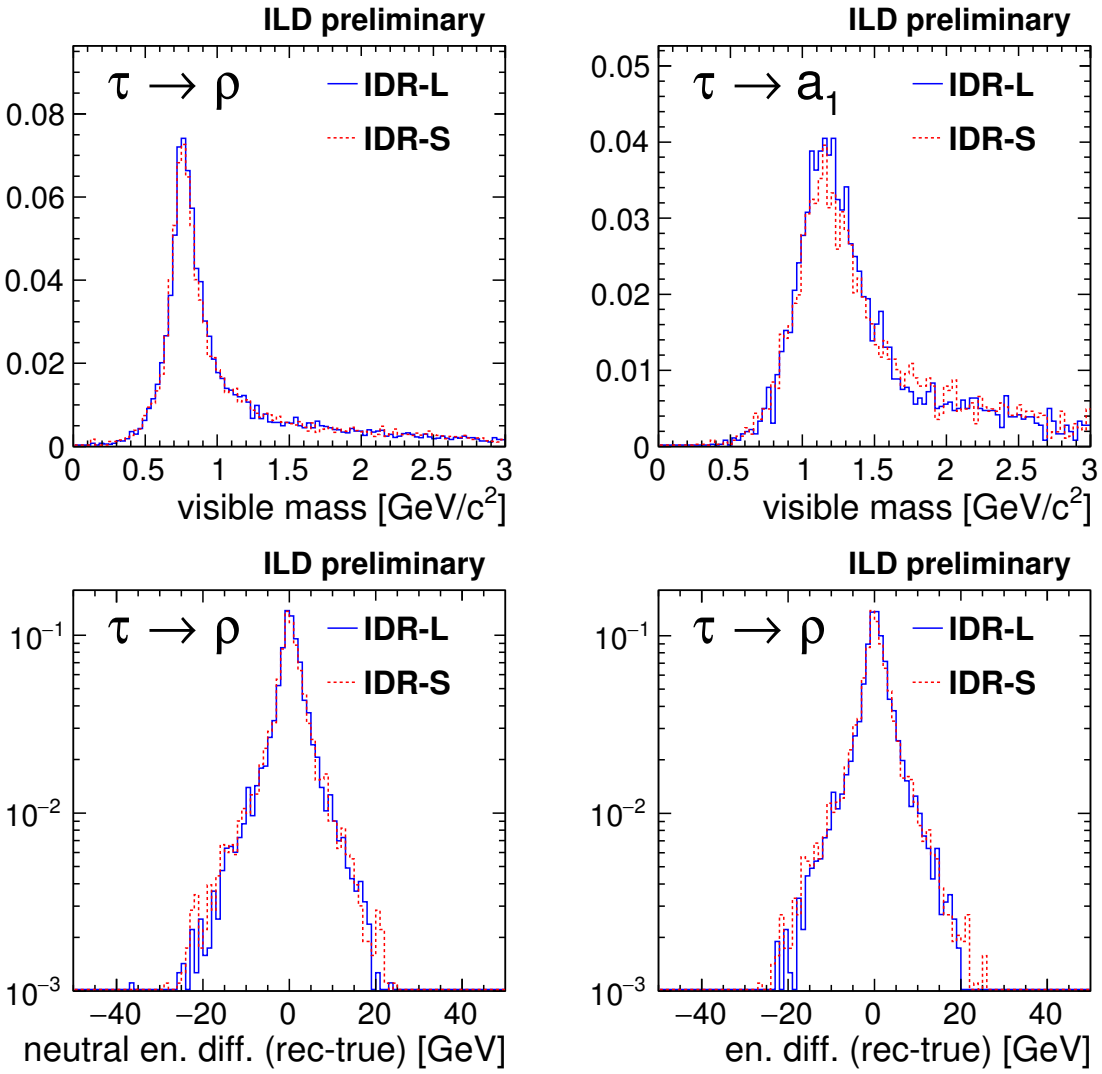

Figure 11: Signal-only comparisons after general event selection. visible invariant mass and the difference between the true and reconstructed visible energy.

ILD_l5_o1_v02	MC-pi	MC-rho	MC-a1p	MC-other	purity
SELECTED AS PI	89.93 ± 0.39	2.04 ± 0.13	0.89 ± 0.14	9.33 ± 0.31	82.34 ± 0.47
SELECTED AS RHO	6.52 ± 0.32	76.25 ± 0.38	12.86 ± 0.51	5.75 ± 0.24	86.99 ± 0.32
SELECTED AS A1P	2.21 ± 0.19	13.27 ± 0.30	65.96 ± 0.72	6.78 ± 0.26	53.69 ± 0.69
ILD_s5_o1_v02	MC-pi	MC-rho	MC-a1p	MC-other	purity
SELECTED AS PI	89.08 ± 0.41	3.21 ± 0.16	1.17 ± 0.17	10.06 ± 0.32	79.21 ± 0.50
SELECTED AS RHO	7.54 ± 0.35	74.59 ± 0.39	17.49 ± 0.59	5.81 ± 0.25	84.70 ± 0.34
SELECTED AS A1P	2.20 ± 0.19	14.14 ± 0.31	59.59 ± 0.76	6.31 ± 0.25	50.11 ± 0.71

Table 2: Selected 1-prong tau candidates in signal events: decay mode identification efficiency in large and small models (unpolarised sample), and the purity considering only backgrounds from the signal process.

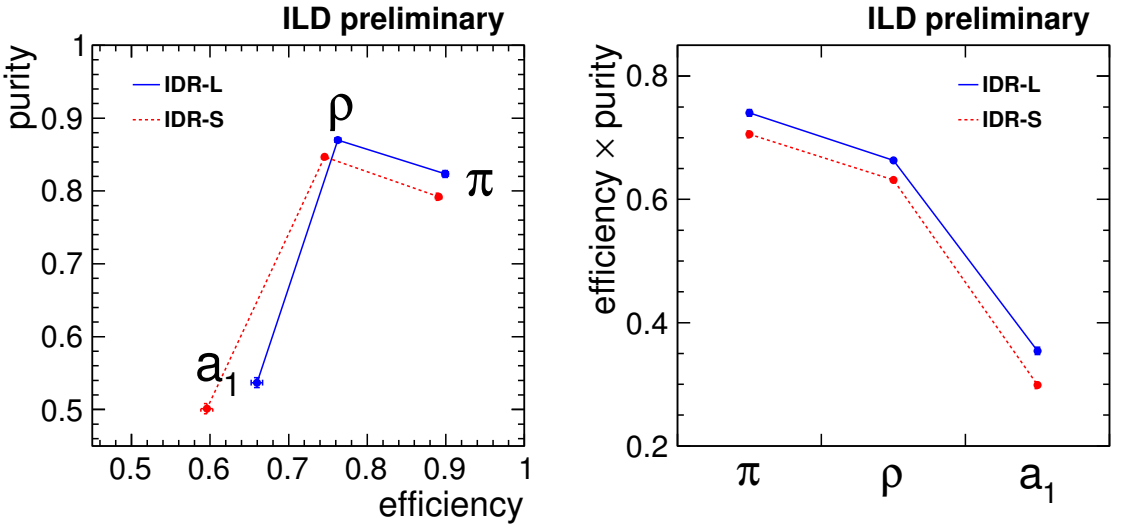

Figure 12: Separation of single prong tau decay modes: the efficiency and purity (left) and their product (right) of the decay mode selection described in the text. The purity definition includes only other high mass di-tau events as background.

4 Tau decay mode selection

To decide whether a jet originates from $\tau^{\pm} \to \pi^{\pm}\nu$ or $\tau^{\pm} \to \pi^{\pm}\pi^{0}\nu$, we first require that it contains a single charged PFO. A cut-based selection is based on 3 observables of particles in the trimmed candidate jet:

- number of identified photon PFOs,
- total invariant mass of all visible particles, and
- total invariant mass of all neutral visible particles.

The same selection criteria are used in both detectors models. The performance of this identification in both models is shown in table 2 and summarised graphically in Fig. 12.

As shown in both the table and the plot, the performance of the large detector model is somewhat better than the small one, with slightly better efficiency and/or purity when selecting these three decay modes.

5 Polarimeter estimation

We here discuss how to extract polarisation information from measurements of the tau decay products.

In the present analysis, we adopt an approach which makes use of only the visible 4-vectors of the charged (and potentially neutral) pions produced in the tau decay, as described in [1]. We use just the pi and rho decays. In the case of the pi, we use just the energy of the pion, while rho decays make use of a much more complicated function of the measured momenta, as described in the above reference.

In fig 13 we show the signal-only reconstructed polarimeters in the two detector models and for 100% polarisation scenarios, and their difference to the MC truth, for tau jets whose decay has been correctly identified, in selected events. The shapes of the distributions clearly show differences, and some small differences between detector models are visible.

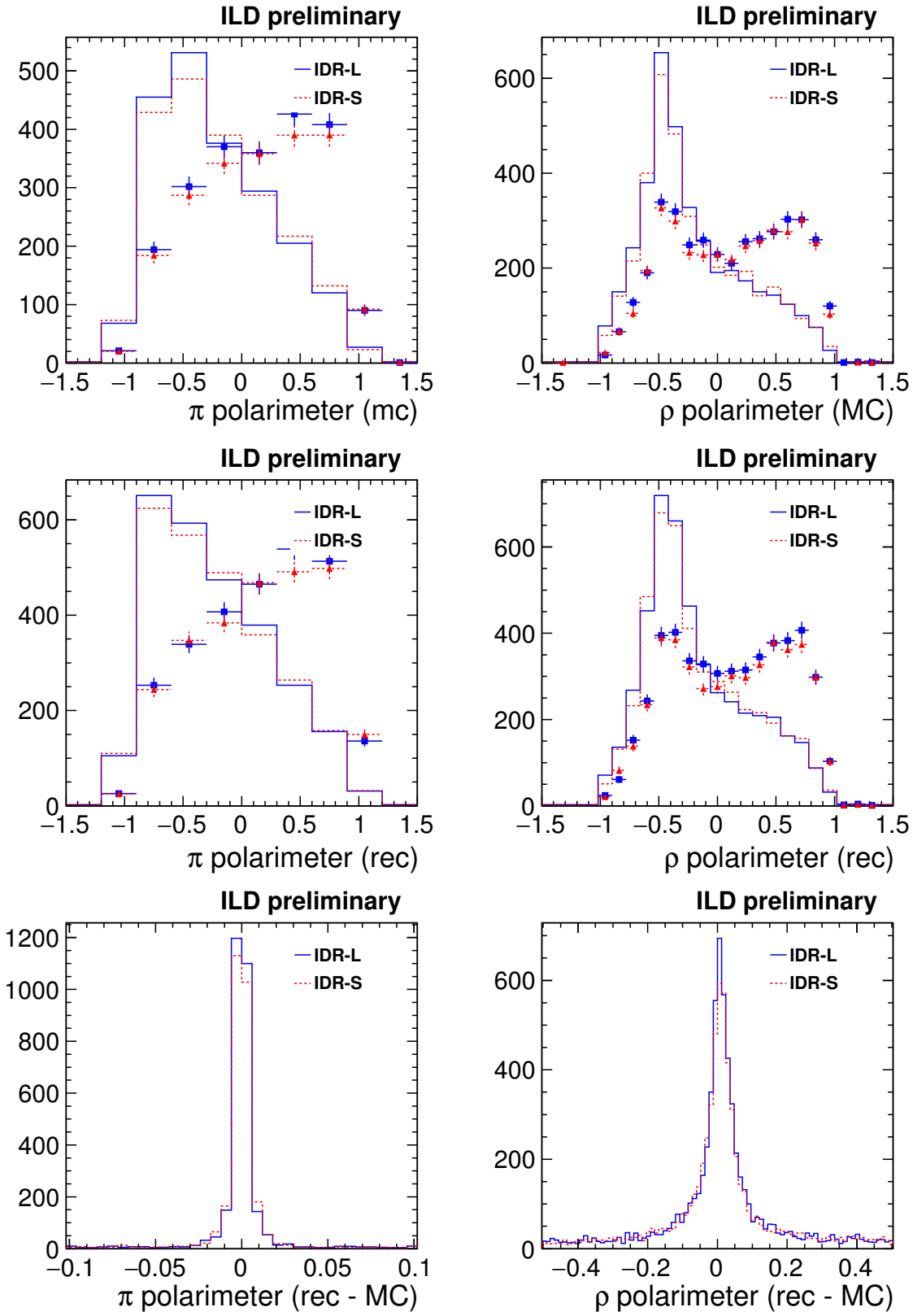

Figure 13: Polarimeters in selected and correctly identified taus. Top: distributions of the true polarimeters for jets in selected signal events: the full line histograms are for 100% eLpR beam polarisation, and the markers with error bars are for 100% eRpL polarisation. Middle: the same for the reconstructed polarimeters. Bottom: the jet-by-jet difference between the reconstructed and true polarimeter values.

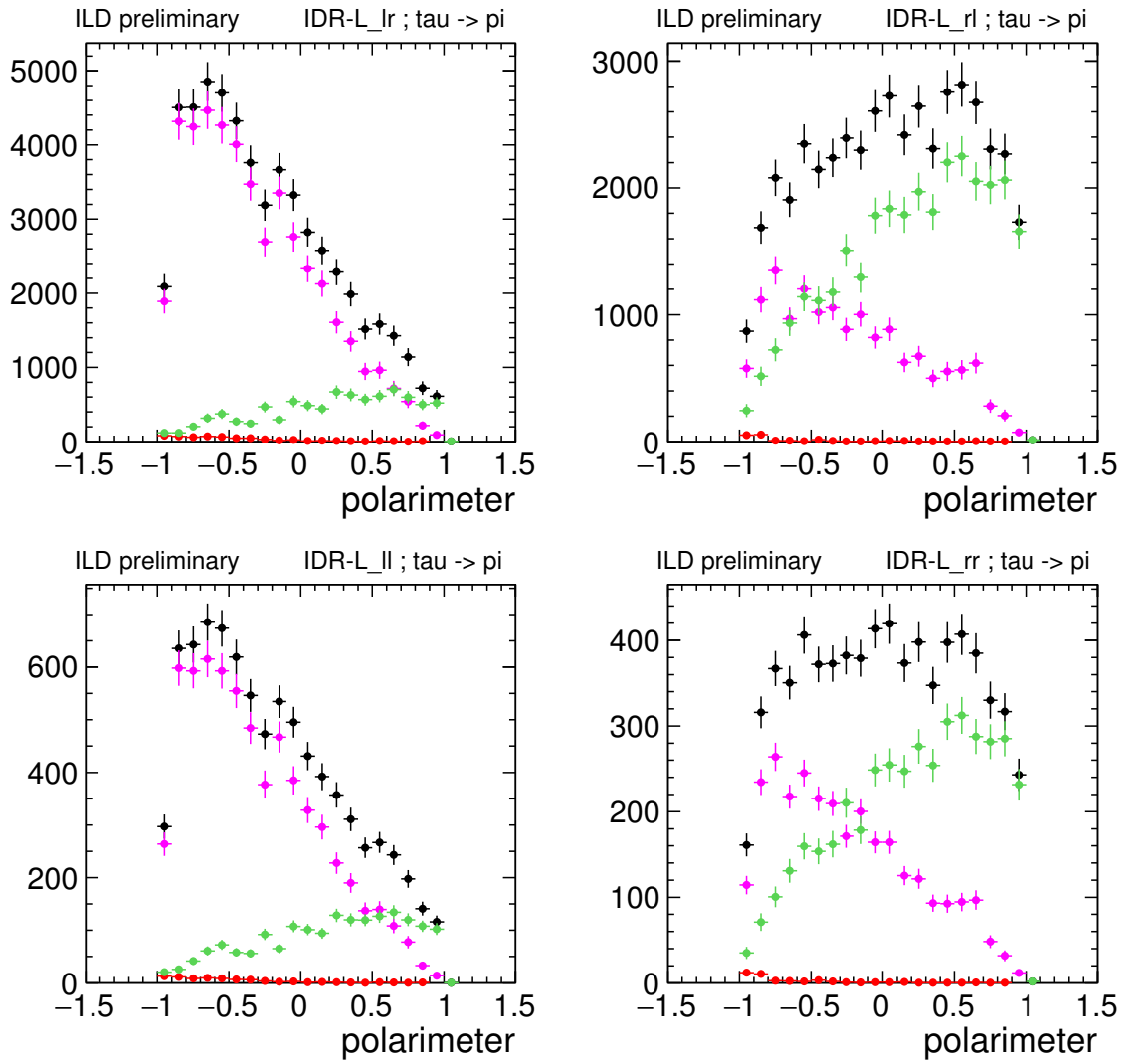

Figure 14: Polarimeter templates for $\tau \to \pi$ decays, scaled to the expected integrated luminosity in the four polarisation scenarios. Black=total, pink=negative hel, green=positive hel, red=background. Error bars are due to finite MC statistics, which were ignored when estimating the measurement precision. IDR-L detector model.

We use the reconstructed polarimeter distributions to run a series of pseudo-experiments to estimate the precision with which we can estimate the fraction of positive and negative helicity taus produced in the sample. We assume that the helicity fractions in the tau-tau samples are independent of energy, and assume that the background distributions are known exactly. The resulting distributions, normalised to the expected integrated luminosity, are shown in figs 14, 15 for each of the four polarisation combinations (assuming 80/30 beam polarisation) in the two considered tau decay modes.

These templates were used to run a series of pseudo-experiments, which were then fitted to extract the fraction of taus in the negative helicity state. The precision on the determination of this fraction (the mean of the distribution of parameter fit errors in the ensemble of pseudo-experiments) are shown in table 3. The two decay modes have rather similar precision, the smaller statistics of the pion mode being compensated by its greater per-event distinguishing power. There is no clear advantage for either of the two detector models. The differences seen in the various measurements, which when seen together do not favour any particular model, are likely due to MC statistics of the fit templates.

5.1 Fancy methods which don't (yet) work very well

In the case of single pion decay, the optimal polarimeter is very simple: the ratio of the pion energy to the beam energy (assuming that the taus are exactly back-to-back). In the case of rho decay, full sensitivity to the tau lepton polarisation requires reconstruction of the neutrino momenta. Attempts were made to use and develop such methods, which so far achieved only limited success. We report on them for completeness.

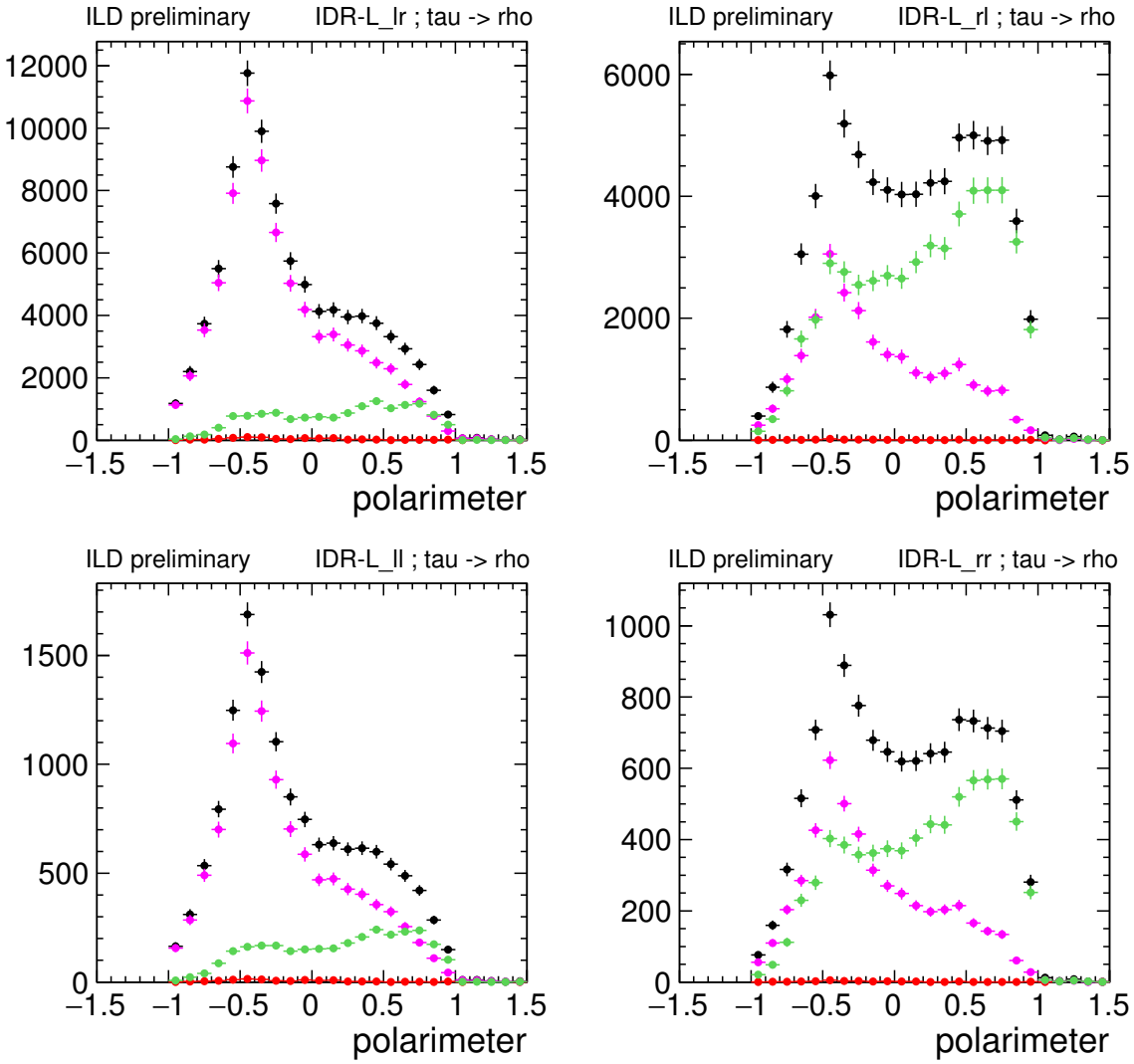

Figure 15: Polarimeter templates for $\tau \to \rho$ decays, scaled to the expected integrated luminosity in the four polarisation scenarios. Black=total, pink=negative hel, green=positive hel, red=background. Error bars are due to finite MC statistics, and are ignored when estimating the measurement precision. IDR-L detector model.

		Precision on helicity fraction [%]						
		$\tau \to \pi$			$\tau \to \rho$			
Beam Pol.	Int. Lum.	MC	fullsim		MC		fullsim	
80/30	4/ab	exact	IDR-L	IDR-S	exact	approx	IDR-L	IDR-S
eLpR	40%	0.283	0.365	0.386	0.190	0.243	0.360	0.346
eRpL	40%	0.329	0.469	0.461	0.218	0.306	0.439	0.471
eLpL	10%	0.773	1.005	1.040	0.518	0.657	0.963	0.941
eRpR	10%	0.874	1.214	1.202	0.581	0.780	1.117	1.172

Table 3: Results of polarimeter fits: uncertainty on the helicity fraction, in %. "Exact" MC results assume 100% efficiency, 0 background, and use MC information to reconstruct the exact polarimeters. "Approx." MC results in the rho channel instead use the approximate extraction of polarimeters, without using the neutrino momentum. The "winner" in the L-S competition in each category is highlighted in colour.

In the case of back-to-back taus of known energy, the neutrino momenta can be estimated by constraining the tau lepton energies (250 GeV), their being back-to-back, and imposing the known tau mass. Zero or two (possibly identical) solutions occur, which correspond to the momentum lying along intersection of 2 cones around the visible tau momenta. It is not clear to me how to choose between these 2 solutions. In events with only pi and rho decays, a good solution was found in only around one third of events.

An alternative method is based on the impact parameter of the charged particles, as described in [2] and used in [3]. We know that the tau must decay somewhere on the charged particle's trajectory. If we know the IP position, we can therefore constrain the tau momentum to lie in the plane defined by the trajectory and the IP. In the events discussed here, the IP cannot be directly measured, since no prompt tracks are produced in the reaction. However, the small ILC interaction region provides a strong constraint in the transverse plane. To estimate the position in z, we simply take the average of the tau jet seeds' z0 track parameters. Better results may come from scanning along z, and finding the "best" solution, or by requiring a multi-prong decay of one of the taus in an event. By assuming a single neutrino per tau decay and imposing the tau mass, we find neutrino momenta which result in positive tau decay lengths and minimise the pT of the tau-tau system. Using this method, again only about a third of events could be reconstructed.

In the future, it would be interesting to combine elements of these two methods, which will hopefully result in a more robust technique for fully reconstructing the tau momentum.

6 Conclusion

Acknowledgments

References

[1] L. Duflot, "Nouvelle méthode de mesure de la polarisation du τ. Application au canal $\tau \to a_1 \nu_\tau$ dans l'expérience ALEPH.," LAL-93-09.

[2] D. Jeans, "Tau lepton reconstruction at collider experiments using impact parameters," Nucl. Instrum. Meth. A **810**, 51 (2016)

[3] D. Jeans and G. W. Wilson, "Measuring the CP state of tau lepton pairs from Higgs decay at the ILC," Phys. Rev. D **98**, no. 1, 013007 (2018)